ACS central science

http://pubs.acs.org/journal/acscii

Research Article

Instant Adhesion of Amyloid-like Nanofilms with Wet Surfaces

Rongrong Qin,[#] Yishun Guo,[#] Hao Ren, Yongchun Liu, Hao Su, Xiaoying Chu, Yingying Jin, Fan Lu, Bailiang Wang,* and Peng Yang*

Cite This: *ACS Cent. Sci.* 2022, 8, 705–717

Read Online

ACCESS | Metrics & More | Article Recommendations | Supporting Information

ABSTRACT: The adhesion and modification of wet surfaces by an interfacial adlayer remain a key challenge in chemistry and materials science. Herein, we report a transparent and biocompatible amyloid-like nanofilm that breaks through the hydration layer of a wet surface and achieves strong adhesion with a hydrogel/tissue surface within 2 s. This process is facilitated by fast amyloid-like protein aggregation at the air/water interface and the resultant exposure of hydrophobic groups. The resultant protein nanofilm adhered to a hydrogel surface presents an adhesion strength that is 20 times higher than the maximum friction force between the upper eyelid and eyeball. In addition, the nanofilm exhibits controllable tunability to encapsulate and release functional molecules without significant activity loss. As a result, therapeutic contact lenses (CLs) could be fabricated by adhering the functionalized nanofilm (carrying drug) on the CL surface. These therapeutic CLs display excellent therapeutic efficacy, showing an increase in cyclosporin A (CsA) bioavailability of at least 82% when compared to the commercial pharmacologic treatment for dry eye syndrome. Thus, this work underlines the finding that the bioinspired amyloid-like aggregation of proteins at interfaces drives instant adhesion onto a wet surface, enabling the active loading and controllable release of functional building blocks.

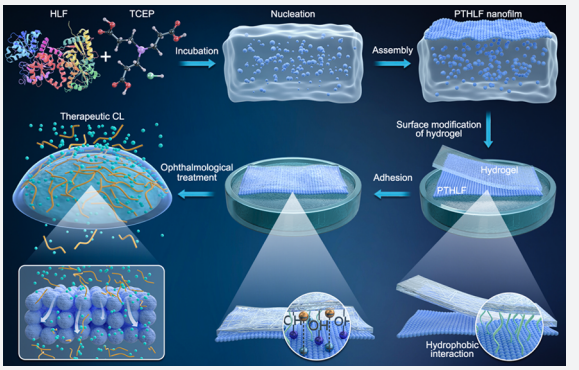

INTRODUCTION

Dry materials can be effectively adhered by an interfacial layer through intermolecular forces, such as hydrogen bonding, electrostatic, and van der Waals interactions.[1,2] However, such modification is challenging to wet material surfaces, such as hydrogels and tissues, because water separates the molecules of the coating and wet material surface and prevents the interactions that are necessary for durable adhesion.[3] This bottleneck noticeably restricts the development and application of hydrogels, since the grafting of a functional layer on hydrogels would greatly expand their general applicability in many important fields, such as drug delivery,[4,5] biomedical devices,[6−8] tissue engineering,[9,10] stretchable and biointegrated electronics,[11,12] and soft robotics.[13] Although it is currently possible to modify a hydrogel surface by graft polymerization on a hydrogel framework,[4,14,15] this confined interfacial modification suffers from several limitations: complex reaction, uncontrollable thickness of the coating, low biological compatibility, and requirement for active sites on the surface (e.g., a surface covered by amine groups).[4,5,15−17] In this regard, a general and moderate method to modify wet material surfaces with rapid reaction speed, low toxicity, and simple functionalization procedures is still a critical demand and central challenge in the field of current material and chemical science.

In contrast to this synthetic dilemma, creatures in nature have already broken through the hydration layer of a wet surface, allowing themselves to achieve stable adhesion. For instance, barnacles utilize a system of amyloids to develop stable waterborne adhesion on solid surfaces.[18] Inspired by this observation, herein, we report a one-step, instant (within 2 s) and nontoxic approach to modify wet material surfaces with a proteinaceous nanofilm, which is based on amyloid-like protein aggregation formed under ambient conditions in a neutral aqueous solution.[19−21] The hydrophobic amino acid residues exposed during amyloid-like protein aggregation at the air/water interface can displace the thin hydration layer of a hydrogel surface, which facilitates fast multiplex interactions between the proteinaceous nanofilm and wet surface. Based on this conceptual progress, we further utilize this strategy to develop functional therapeutic contact lenses (CLs) for dry eye syndrome (DES) treatment. We chose human lactoferrin (HLF), a defensive protein in the human immunology system, and adhered HLF nanofilms onto the hydrogel CL surface by

Received: February 9, 2022
Published: June 1, 2022

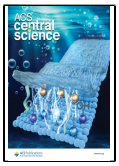

manipulating the amyloid-like aggregation of HLF. HLF, generally recognized as a safe material by the US Food and Drug Administration (FDA), is commercially available at low cost from human colostrum and other external secretions, such as tears, saliva, and semen.[22−24] The present work then proves that the amyloid-like aggregation of HLF not only shows robust adhesion on a variety of hydrogel materials but also contains space to allow for the controllable encapsulation/release of functional molecules. In this way, a functionalized CL coated with a cyclosporin A (CsA)-loaded HLF nanofilm exhibits a controllable release of CsA when applied to eyes, which improves the CsA bioavailability by at least 82% when compared to that of Restasis, a commercial CsA emulsion that is currently the only pharmacologic treatment for DES approved by the US FDA.[25] This finding would open a window to utilize a family of protein amyloids in wet surface modification. Moreover, since DES affects approximately one-third of people globally,[26] and the major challenge of DES treatment is to slow down the release of CsA and enhance its bioavailability in ocular treatments, our results to improve CsA bioavailability by 82% demonstrate the great potential of amyloid assembly in the development of smart functionalized CLs for ophthalmology treatment.

RESULTS

Structure and the Adhesion Mechanism of the Phase-Transitioned HLF Nanofilm. The way to manipulate amyloid-like aggregation of HLF is a method termed protein phase transition, in which the intramolecular disulfide bonds of a protein are reduced to trigger the transformation from a soluble native protein phase to insoluble protein aggregates (Figure 1A).[19−21] In the present work, after mixing HLF

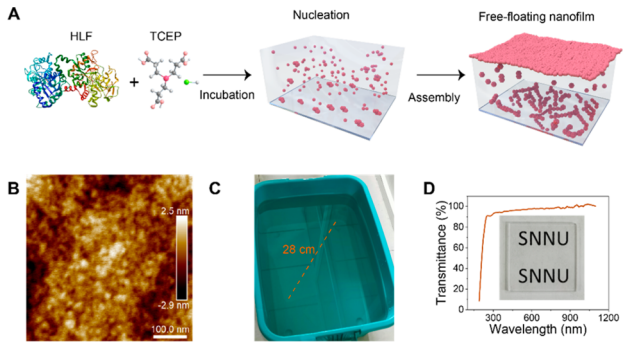

Figure 1. Macroscopic PTHLF nanofilm floating at the air/water interface and its formation mechanism. (A) Schematic illustration of the PTHLF film formed at the air/water interface and ambient temperature by mixing HLF and TCEP in water. (B) AFM image of the film. (C) Photograph of a film floating on Milli-Q water. (D) Optical transparency of the film coated on quartz glass. The inset image shows the corresponding photograph.

aqueous solution with a solution of tris(2-carboxyethyl) phosphine (TCEP), a disulfide reductant in a pH range of 5−12 (Figure S1) at room temperature, HLF aggregated rapidly to form 20−25 nm oligomer nanoparticles, as reflected by atomic force microscopy (AFM) (Figure 1B). These oligomer nanoparticles further evolved into two pathways: agglomeration at the air/water interface to form a floating protein nanofilm and continuous growth into microparticles in bulk solution (Figure 1A). The higher the HLF concentration was, the faster the protein aggregation. Typically, a size distribution increase from 15 nm to 10 μm was observed in the system from 5 to 60 min, as reflected by dynamic light scattering (DLS) (Figure S2). As a defensive protein in the human immunology system, the killing capability toward the typical Gram-positive bacterium *Staphylococcus aureus* (*S. aureus*) of native HLF was highly preserved after the phase transition (Figure S3). This indicated that the highly alkaline N-terminal region of HLF, which determines the biological functions of HLF, might not be largely disturbed during the phase transition.[22] The nanofilm area was well regulated by adjusting the area of the air/water interface, and a phase-transitioned HLF (PTHLF) nanofilm as large as 400 cm^2 was easily acquired at the laboratory scale (Figure 1C). The PTHLF nanofilm was colorless and displayed excellent optical transparency (as high as ∼100%) between 300 and 800 nm, thereby behaving as a unique class of stealth coating that is very useful in optical applications (Figure 1D). As further analyzed by AFM profiling, by simply controlling the incubation time (Figure S4) and pH of the TCEP solution (Figure S5), the thickness of the nanofilm could be easily modulated from 15 to 70 nm, and the root-mean-square (RMS) of the nanofilm to reflect the surface roughness, only varied from 1 to 9 nm, indicating that the surface of the nanofilm is very smooth. As in previous research results, the hydrophobic interactions provided an important driving force to facilitate the aggregation of proteins.[27] In the presence of ANS, a staining sensitively detects the exposure of hydrophobic groups, the corresponding fluorescence intensity at 475 nm of the mixture of HLF and TCEP rapidly increased in ∼60 min, and the higher the pH, the faster the fluorescence intensity increased, namely, the faster the protein aggregation (Figure S6A). Upon unlocking the intramolecular disulfide bonds in the phase transition, the high-energy α-helix of native HLF was rapidly unfolded and aggregated into β-sheet stacking, as further confirmed by the thioflavin T (ThT) staining (Figure S6B,C), attenuated total reflectance Fourier transform infrared (ATR-FTIR) spectroscopy (Figure S7A), and far-UV circular dichroism (CD) (Figure S7B) findings.[19,28] These results implied the existence of amyloid-like structures in the PTHLF nanofilm.

The amyloid-like structure is an important building block for bioadhesion on surfaces in nature.[21,29−32] Although the detailed mechanism for amyloid-mediated adhesion on a solid surface has not been completely clear until now, it is believed that functional groups contribute largely to interfacial adhesion through the formation of multiplex interactions with a surface.[33] Compared with dry materials, the adhesion of amyloids on wet hydrogels is more complicated, since the structure must first break through the hydration layer on the hydrogel surface before interacting with the molecular framework of the hydrogel.[34,35] In this regard, the PTHLF nanofilm may fulfill these requirements. The high-resolution X-ray photoelectron spectroscopy (XPS) of C_{1s} indicated a variety of chemical structures existing on the nanofilm surface (Figure S8). The multiple functional groups of the PTHLF film were from the versatile hydrophilic and hydrophobic amino acid residues of amyloid-like protein aggregates, which was consistently confirmed by the deconvolution of the Raman spectra to show the increased propensity of Trp, tyrosine (Tyr), phenylalanine (Phe), cysteine (Cys), and NH_2^+/NH_3^+ in the PTHLF nanofilm (Figure S9A−C and Table S1). The versatile chemical groups on the nanofilm surface supported the co-contribution from coordination bonds, hydrogen bonds,

https://doi.org/10.1021/acscentsci.2c00151
ACS Cent. Sci. 2022, 8, 705−717

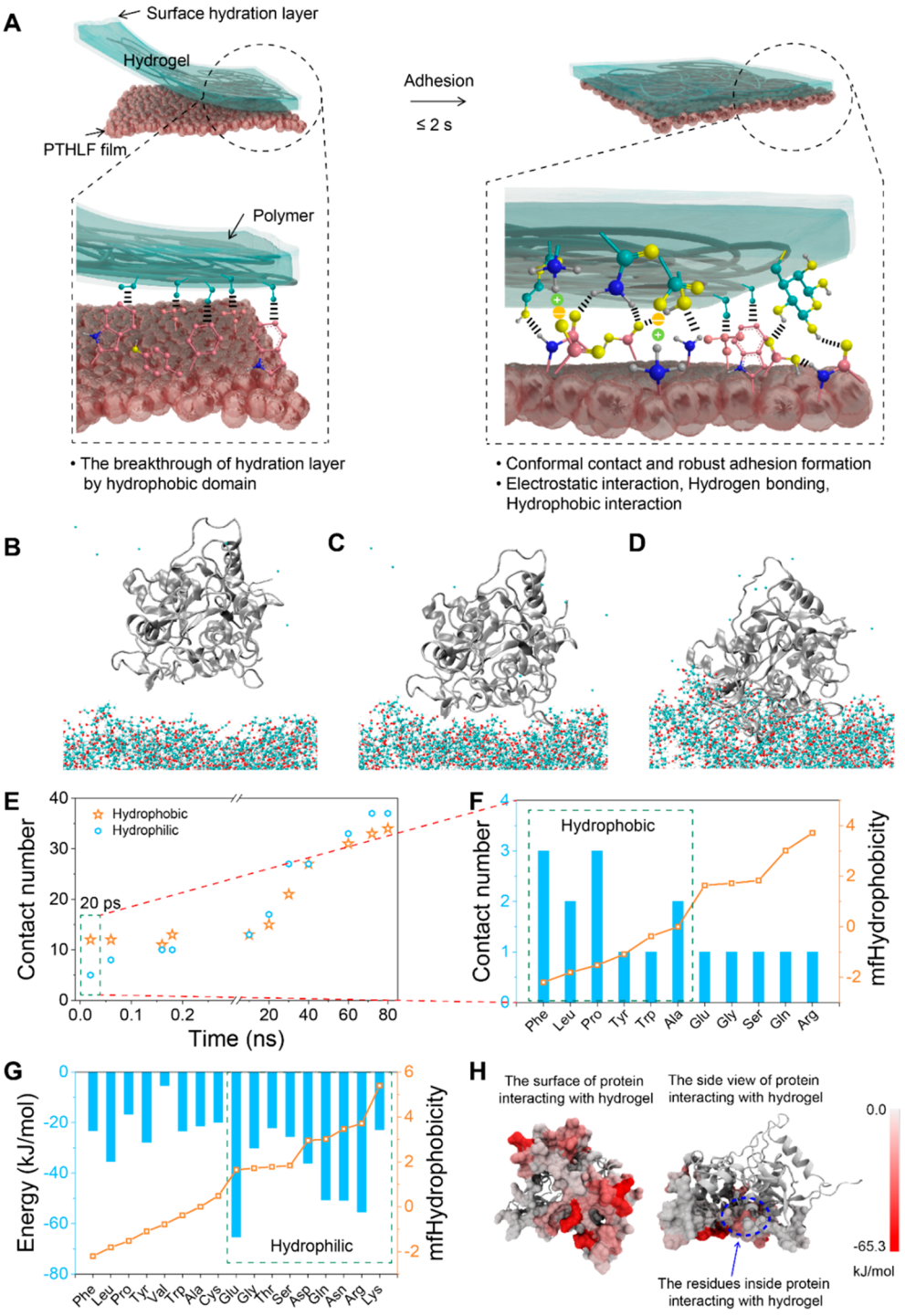

Figure 2. Adhesion mechanism between the PTHLF nanofilm and hydrogel. (A) Schematic showing the interaction between the PTHLF nanofilm and hydrogel. Representative snapshots of PTHLF (at air/water interface) adhesion on the PHEMA hydrogel at (B) 0 ns, (C) 0.02 ns, and (D) 80 ns. (E) Number of hydrophobic and hydrophilic residues in contact with the PHEMA hydrogel as a function of time. (F) Number of residues in contact with the PHEMA hydrogel at 0.02 ns (20 ps). (G) Maximum energy of different residues interacting with the PHEMA hydrogel at 80 ns. (H) Energy distribution of the PTHLF residues interacting with the PHEMA hydrogel.

and electrostatic and hydrophobic interactions with the material, regardless of the chemical composition of the material surface.[21,29,33] In particular, hydrophobic structures were noticeably present on the PTHLF nanofilm, as the C_{1s} signal of the aliphatic carbon (C−H/C−C) groups had a weighted contribution of over 43.89% among all the carbon-derived structures on the PTHLF nanofilm (Figure S8B). In contrast, this signal was 26.90% in native HLF (Figure S10), and the corresponding propensity of hydrophobic Trp residues in PTHLF was 1.5 times higher than that in native HLF (Figure S9C). The exposure of these hydrophobic groups was consistent with hydrophobicity-induced aggregation occurring during the protein phase transition (Figure S6A), which facilitated the depletion of water molecules on a hydrogel surface by the hydrophobic side chains of proteins.[36−38] After that, the abundant functional groups on the PTHLF nanofilm

https://doi.org/10.1021/acscentsci.2c00151
ACS Cent. Sci. 2022, 8, 705−717

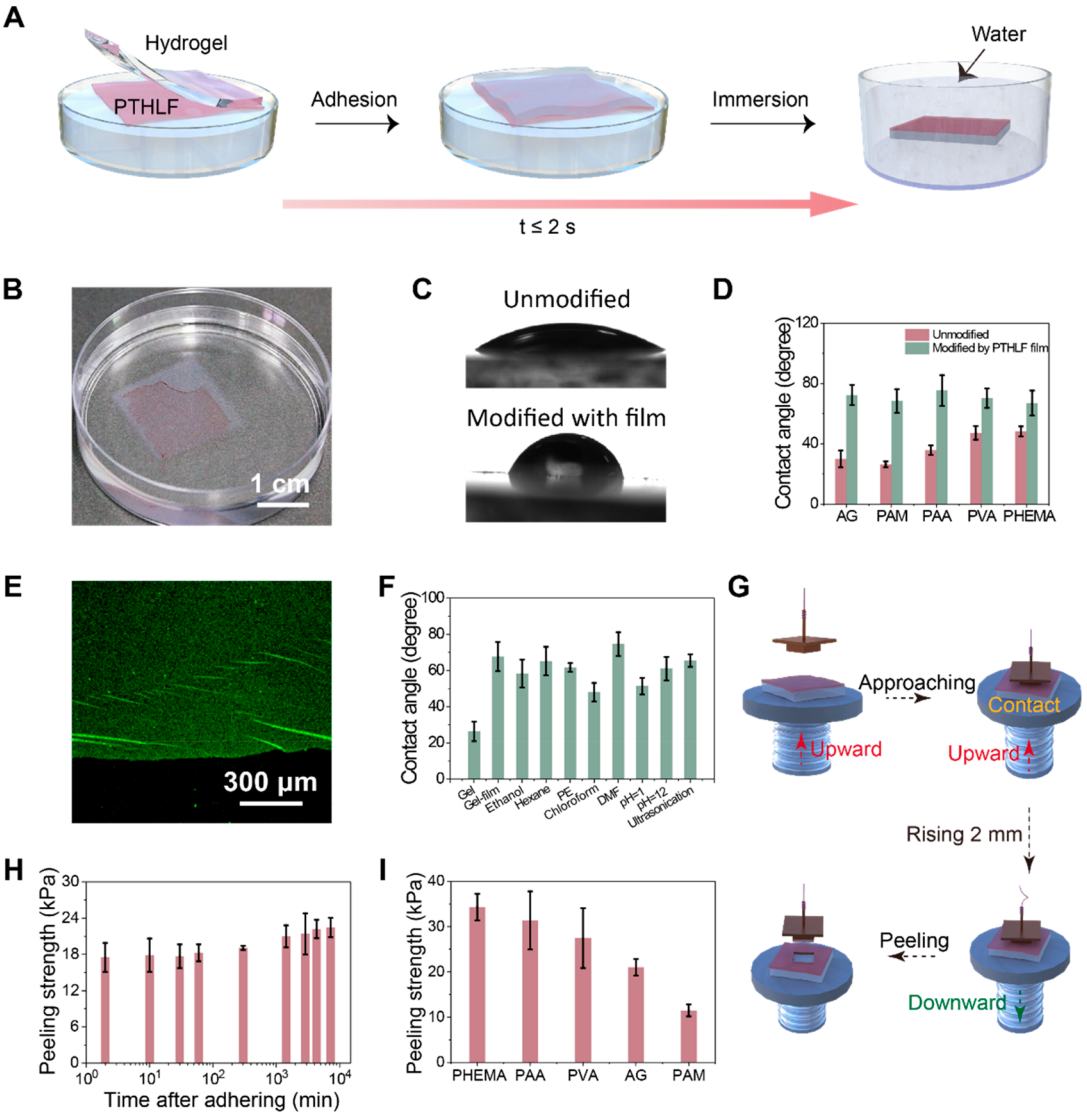

Figure 3. Various PTHLF film-modified hydrogels and the peeling strength between the film and hydrogels. (A) Schematic illustration of the process of the PTHLF film modifying the hydrogel surface. (B) Photograph of the dyed PTHLF film-coated agarose hydrogel after immersion in Milli-Q water. (C) Pictures of the water droplets on bare agarose hydrogel and the PTHLF film-coated agarose hydrogel. (D) Water contact angles on the different PTHLF film-coated hydrogels. (E) LSCM image of the agarose hydrogel modified with the PTHLF film dyed by ThT. (F) Water contact angle on the PTHLF film-coated agarose hydrogel treated with organic solvents, extreme pH conditions, and ultrasonication. (G) Scheme of the peeling strength measurement process. (H) Peeling strength versus time after adhering the PTHLF film on the agarose hydrogel. (I) Peeling strength between the different hydrogels and PTHLF film. Values represent the mean and standard deviation (n = 3−5). The typical conditions of PTHLF film formation were 7 mg/mL HLF, 50 mM TCEP at pH 6.98, and incubation for 2 h.

could then reach the interactive distance for multiplex intermolecular interactions (Figure 2A).

The above deduction was then supported theoretically by molecular dynamics (MD) simulations. MD simulation of native HLF after cleavage of the S−S bonds for 2.8 μs indicated that the structure of unfolded HLF was looser than that of native HLF (Figure S11A−C). As a result of unfolding, except for proline (Pro), the solvent-accessible surface area (SASA) of most hydrophobic and hydrophilic amino acid residues increased (Figure S11D). MD simulation of the unfolded HLF in solution for 25 ns then proved that the unfolded HLF would spontaneously move to the air/water interface (Figure S12A−C). At the air/water interface, the unfolded protein further underwent a significant conformational change from a random coil to a β-sheet (Figure S12D), which was consistent with the experimental results of amyloid-like structures in the nanofilm. The decrease in the SASA of HLF indicated that the structure of the unfolded HLF became tighter after assembly at the air/water interface compared to the loose unfolded structure in the solution, and the hydrophilic residues tended to be more buried in the protein molecule than the hydrophobic residues (Figure S12E,F). In particular, more hydrophobic residues in the unfolded HLF were exposed at the air/water interface (Figure S12G,H), which was consistent with the XPS and Raman spectroscopy results showing enriched hydrophobic residues on the PTHLF nanofilm. The surface of protein at the air/water interface was plate-like, which provided more interaction sites for the adhesion of the protein with substrates (Figure S12G). The adhesion ability of HLF assembled at the air/water interface was then simulated by initially placing the assembled HLF 5 Å away from the surface of the polyhydroxyethyl methacrylate

https://doi.org/10.1021/acscentsci.2c00151
ACS Cent. Sci. 2022, 8, 705−717

(PHEMA) hydrogel (Figure 2B and Figure S13A). The simulation trajectories then indicated that the protein at the air/water interface could stably adsorb on the PHEMA hydrogel (Figure 2C,D and Figure S13B−D). As the adsorption proceeded, the number of contact residues and hydrogen bond gradually increased, while van der Waals force and electrostatic interactions were more energetically favorable (Figure 2E and Figure S13E,F). It should be noted that the contact number of hydrophobic residues was 2.4 times higher than that from hydrophilic residues at the beginning 20 ps, which proved that hydrophobic interactions were dominant at the initial stage of protein interaction with the PHEMA hydrogel (Figure 2E,F). Then, the number of hydrophilic contact residues increased, while the number of hydrophobic contact residues remained nearly constant from 20 ps to 10 ns. After that, the number of hydrophobic and hydrophilic contact residues basically increased synchronously; notably, at the end, the number of hydrophilic contact residues was slightly higher. Among the contact residues, the hydrophobic residues Phe, leucine (Leu), Pro, and alanine (Ala) tended to interact with the hydrogel (Figure 2F and Figure S13G). Nevertheless, the interactions of the hydrophilic contact residues with the PHEMA hydrogel were more energetically favorable than those of the hydrophobic contact residues (Figure 2G). The energy distribution diagram of residues of PTHLF interacting with the hydrogel (Figure 2H) and certain interpenetration between PTHLF molecule and PHEMA phase (Figure S13C) indicated that the hydrogel interacted not only with the functional groups on the surface of the protein, but also with residues inside the protein. The results of MD indicated that the adhesion process of PTHLF with a hydrogel can roughly be presented in two steps. At the initial stage (0−20 ps), the hydrophobic groups facilitated the depletion of water molecules on a hydrogel surface by the hydrophobic side chains of proteins. After that, the abundant functional groups on the plate-like PTHLF surface even inside the protein could then reach the interactive distance for multiplex intermolecular interactions with a hydrogel. This co-contribution from versatile chemical groups causes the strong adhesion of PTHLF nanofilm with the hydrogel.

Instant Modification on the Hydrogel Surface by the PTHLF Nanofilm. The MD simulation of the adhesion between the PTHLF and a hydrogel was then experimentally confirmed by transferring the nanofilm onto a variety of common hydrogels, including PHEMA, poly(acrylic acid) (PAA), poly(vinyl alcohol) (PVA), agarose (AG), and polyacrylamide (PAM). Once the transfer occurred, the nanofilm exhibited stable adherence to the hydrogel surface within 2 s (Figure 3A,B and Movie S1). As further directly observed by the field emission-scanning electron microscopy (FE-SEM) images, the nanofilm adhered on all the tested hydrogel surfaces at the microscopic level regardless of the roughness of the hydrogel surface (Figure S14). This result reflected that the nanofilm was flexible enough to support good adaptation to a rough surface, thereby ensuring intimate contact with the substrate. The corresponding ATR-FTIR spectra showed the characteristic amide I and II bands of PTHLF, which reflected the successful coating of the nanofilm on the hydrogels (Figure S15). Redshifts in the bands of the −OH/−NH_2 groups were specifically observed in the ATR-FTIR spectra of the PTHLF nanofilm-coated hydrogels (Figure S15). This result suggested the presence of intermolecular hydrogen bonding between the PTHLF and hydrogels, which averaged the electron cloud density to result in a redshift in the bands of the −OH/−NH_2 groups from the PTHLF and hydrogels.[39,40] After covering the hydrogels with the nanofilm, a noticeable increase in the water contact angle (to ∼70−75°) was observed (Figure 3C,D, Figure S16, and Movies S2−S5). The stealth nanofilm coating was further visually inspected by the staining of Congo red (Figure S17) and ThT dyes (Figure 3E), both of which bind with amyloid structures to induce colorimetric and fluorescent changes, respectively. The nanofilm further exhibited reliable thermostability below 200 °C (Figure S18), as reflected by the thermogravimetric (TG) measurements, and excellent adhesion stability on the hydrogel for sustained treatments under severe conditions, including the presence of organic solvents (e.g., ethanol, hexane, petroleum ether (PE), and dimethylformamide (DMF)), extreme pH values (1−12) and ultrasonication (40 kHz for 30 min) (Figure 3F and Figure S19).

The adhesion strength of the nanofilm to hydrogels was then measured by the peeling test using a self-adapted surface interfacial tension meter (DCAT 21, Dataphysics, Germany) (Figure 3G, Figures S20,21, and Movie S6). We chose AG as the model hydrogel for such evaluation because it is a kind of hydrogel without stickiness. Even so, the PTHLF nanofilm could establish strong adhesion (with a peeling strength of 18 kPa) on the AG hydrogel after being in contact for less than 2 s (Figure 3H, Figure S22, and Movie S1), as the adhesion strength only exhibited a relatively small increase (of less than 20%) in more than 120 h after initial adherence in ∼2 s (Figure 3H). Reliable adhesion strength was further determined for the PTHLF nanofilm adhered to various hydrogels, which was 35 kPa for PHEMA, 32 kPa for PAA, 28 kPa for PVA, and 13 kPa for PAM (Figure 3I and Figure S23). The high adhesion strength ensured the stability of the PTHLF nanofilm coating on the hydrogel in a high shear field, as simulated by subjecting the PTHLF-coated PHEMA hydrogel to strong water flushing at a flow rate of 98.25 ± 2.59 mL/s, which is equal to a force of 10.05 N (Figure S24A−H). After scouring for 24 h, the coating was still stable on the surface of PHEMA, because the water contact angle on the hydrogel was maintained at approximately 70° (Figure S24I). It is known that the maximum friction force between the upper eyelid and eyeball is approximately 0.52 N,[41] which is only one-twentieth of the flushing force of water flow on the PTHLF-coated PHEMA hydrogel during the flushing test. Thus, this result indicated that the PTHLF-coated hydrogel could be applied in eyes without peeling off *in vivo*. The order of adhesion strength of the PTHLF nanofilm on PHEMA, PAA, PVA, AG, and PAM was closely related to the hydration layer on the hydrogel surface. Compared with other hydrogels, PHEMA and PVA hydrogels were more hydrophobic, since the water contact angles on these blank gels were higher than the others (Figure 3D). This implied that compared to those of hydrophilic gels, the nanofilm more easily broke through the hydration layers of the PHEMA and PVA hydrogels to achieve higher adhesion to the hydrogel surface. The penetration through the hydration layer was further supported by freeze-dried nanofilm coated hydrogels (Figure S25). After freeze-drying, it could be seen from the optical picture that the nanofilm still stably adhered to the different polymer hydrogels at the macroscopic level. This indicated that the nanofilm indeed penetrated the hydration layer to interact with polymer chains rather than bonding with a monolayer of water molecules. In this respect, a hydrogel with a high solid content (i.e., low water content),

https://doi.org/10.1021/acscentsci.2c00151
ACS Cent. Sci. 2022, 8, 705−717

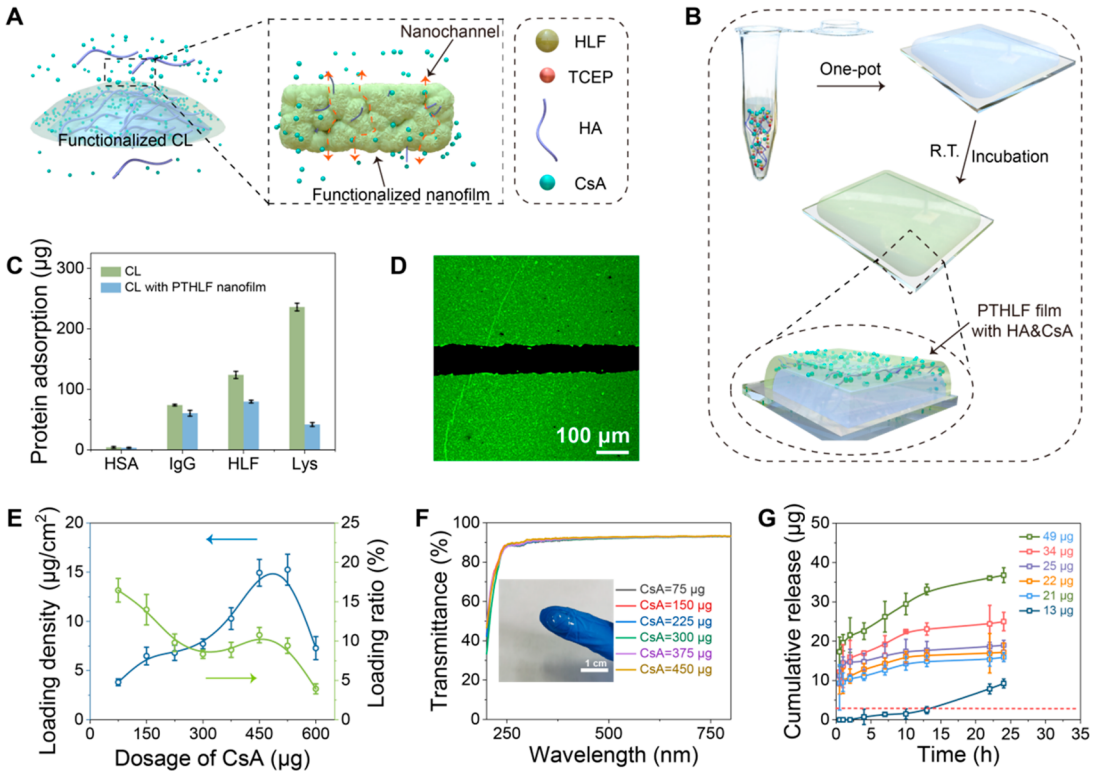

Figure 4. Encapsulation and release of CsA and HA in the PTHLF film. (A) Schematic cartoon showing the release process of functional molecules from the functionalized CL with the PTHLF nanofilm coated. (B) Schematic illustration showing the one-pot encapsulation of CsA and HA in the nanofilm prepared by simply mixing HLF (7 mg/mL in Milli-Q water), TCEP (50 mM in Milli-Q water), CsA (7.5 mg/mL in aqueous ethanol), and a solution of HA and incubating for 12 h at room temperature. (C) Evaluation of the nonspecific adsorption of proteins on the bare and PTHLF-coated CL surfaces (tested by a bicinchoninic acid (BCA) assay). (D) LSCM image of the PTHLF film encapsulating CsA-FITC. (E) Experimental loading density and loading ratio of CsA in the PTHLF film at different feeding doses of CsA. (F) Optical transparency of the functionalized PTHLF film coated on quartz glass. (Inset: a photograph of the functionalized CL). (G) Release curve of the encapsulated CsA from the functionalized film.

such as the PHEMA hydrogel, could support a higher adhesion strength than those hydrogels with high water content (Figure S26).

The adhesion of the PTHLF nanofilm on a hydrogel material could be further extended to other proteins and wet surfaces. First, as discussed above, the adhesion of PTHLF on a hydrogel was mainly based on the large number of hydrophobic domains and multiple functional groups on the nanofilm surface. Such features are basic and common to a few phase-transitioned protein nanofilms, including the phase-transitioned bovine serum albumin (PTB) and phase-transitioned lysozyme (PTL) nanofilms previously reported by our group.[19,21] Thus, these nanofilms could also stably adhere to the hydrogels according to the above procedure (Figure S27). Second, in addition to the hydrogel, the PTHLF nanofilm could also be applied to other wet articles, such as tissues typically including skin, stomach, and muscle (Figures S28 and S29).

Surface Functionalization on CL toward Smart Eye Equipment. As hydrogel materials have been extensively explored in various fields, such as biomedical devices,[14] soft electronics,[42] and drug delivery,[4] the successful adhesion of a protein nanofilm on a hydrogel surface could largely widen the applicability of hydrogels. CL, which is currently worn mainly for vision correction and cosmetic reasons, is one of the most ubiquitous applications of hydrogels. Increasing studies show that CL is a unique platform for wearable electronics[42] or ophthalmic drug delivery systems,[26] because they continue to be in contact with our tear fluids. Nonetheless, the development of functionalized CL is largely restrained, since the methods to modify CL are limited and suffer from the following points: poor biocompatibility, easy influence on the bulk mechanical properties and comfort of the CL, and poor control over the sustainable release of loaded drugs.[43−46] In contrast, PTHLF provided a biocompatible platform to functionalize CL without affecting their bulk properties, such as the Young's moduli (Figure S30). The PTHLF nanofilm adhered to CL could maintain its stability without peeling off or deteriorating after being stored in care solution for at least 1 year (Figure S31). By fully exploring and utilizing the function of the phase-transitioned protein nanofilm toward drug loading and release,[30] a noticeable improvement in DES treatment by PTHLF-coated CL was then demonstrated. DES affects approximately one-third of people globally, and the major challenge of DES treatment is how to slow down the release of symptomatic drugs and to enhance the bioavailability of ocular treatment.[47] For instance, Restasis, currently the only pharmaceutical preparation approved by the US FDA for DES,[25] has a bioavailability of active drug (CsA, a neutral, hydrophobic, cyclic peptide) as low as 1−2%. As a result, with the daily use of CsA at a high dose, only a small fraction of CsA administered by eye drops is typically absorbed into the eye, consequently necessitating multiple doses per day. As the number of eye-drop doses per day increases, so does the potential for ocular surface irritation and systemic side effects (e.g., CsA-induced renal toxicity and gingival overgrowth),

https://doi.org/10.1021/acscentsci.2c00151
ACS Cent. Sci. 2022, 8, 705−717

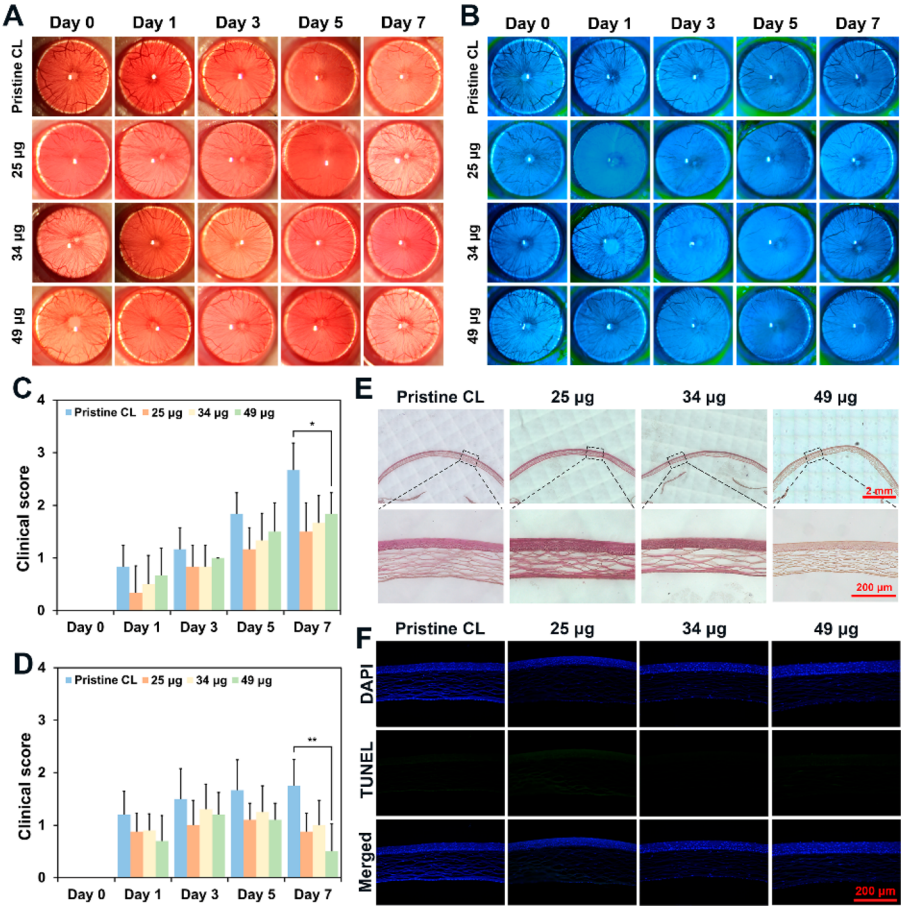

Figure 5. *In vivo* biocompatibility evaluation of the functionalized CL in the eyes of normal SD rats. Representative slit lamp field images (A) and corresponding anterior segment clinical scores (C) of SD rats at 0, 1, 3, 5, and 7 days after various treatments with pristine CL (0 μg) and drug-loaded functionalized CL at different CsA loading doses (25, 34, and 49 μg). Representative images of corneal fluorescein staining (B) and clinical scores (D) at 0, 1, 3, 5, and 7 days after various treatments. (E) Representative immunohistochemical analysis images of corneas at 7 days after various treatments. (F) Representative post-treatment TUNEL staining images of corneas at 7 days after various treatments. Statistical significance: $p < 0.01$ (*), $p < 0.001$ (**), $p < 0.0005$ (***), $p < 0.0001$ (****).

while patient compliance with the treatment regimen decreases.[26] As demonstrated below, the advantage of PTHLF-coated CLs is in their efficient encapsulation and controllable release of CsA, which directly increases the bioavailability of CsA by 82%.

The encapsulation and release of drugs by the PTHLF nanofilm is based on the nanochannels formed among the close-packing protein oligomeric nanoparticles.[30,48] These voids provide physical space to hold external molecules, and when the size of the functional molecules is equal to or smaller than the space size, the entrapped molecules can then be slowly released through the channels (Figure 4A).[30,48] As tested by the Brunauer-Emmet-Teller (BET) method, the pore size distribution of the PTHLF nanofilm was 1.5−1.7 nm (Figure S32A,B), which was almost equal to the size of CsA at 1.8 nm (Figure S32C). The one-pot encapsulation of CsA in the nanofilm was then initiated by mixing HLF, hyaluronic acid (HA), TCEP, and CsA at given concentrations (Figure 4B), and the resultant functionalized PTHLF nanofilm was coated onto a commercial disposable CL to produce a therapeutic CL for DES. The reason for supplying HA in this formula is that HA is a natural moisturizer and antifouling agent, which directly reduces the water evaporation of the hydrogel by 20% (Figure S33) and suppresses the nonspecific adsorption of bacteria such as *S. aureus* (Figure S34) and lacrimal proteins by 58% (Figure 4C and Figure S35). In the corresponding FE-SEM images, hydrophobic CsA particles were clearly observed on the treated nanofilm (Figure S36). A direct visualization of CsA or HA encapsulation was further shown by entrapping FITC-labeled CsA (CsA-FITC) or HA (HA-FITC) in the nanofilm, as demonstrated by the laser scanning confocal microscopy (LSCM) images (Figure 4D and Figures S37 and S38). In contrast, the control sample obtained by simply immersing the nanofilm in the CsA-FITC or HA-FITC solution did not lead to noticeable fluorescence (Figures S37 and S38). The maximum encapsulation densities of CsA and HA in the nanofilm were 15 and 0.55 $\mu g/cm^2$, respectively (Figure 4E and Figure S39). The difference in the encapsulation density between CsA and HA may be due to the large difference in the molecular weight and hydrophilicity of the two molecules; additionally, the hydrophobic groups exposed during the assembly and formation of the PTHLF nanofilm were beneficial for the inclusion of the hydrophobic drug CsA. Based on the surface area of a CL, the maximum encapsulation amount of CsA in a PTHLF nanofilm-coated CL could be up to ~95 μg. This value is 5 times higher than the maximum encapsulation of CsA in a commercial CL by simple immersion of the CL in CsA solution (Figure S40). Even when packed with functional molecules, the nanofilm still maintained an optical transparency as high as ~92% between 400 and 700

https://doi.org/10.1021/acscentsci.2c00151
ACS Cent. Sci. 2022, 8, 705−717

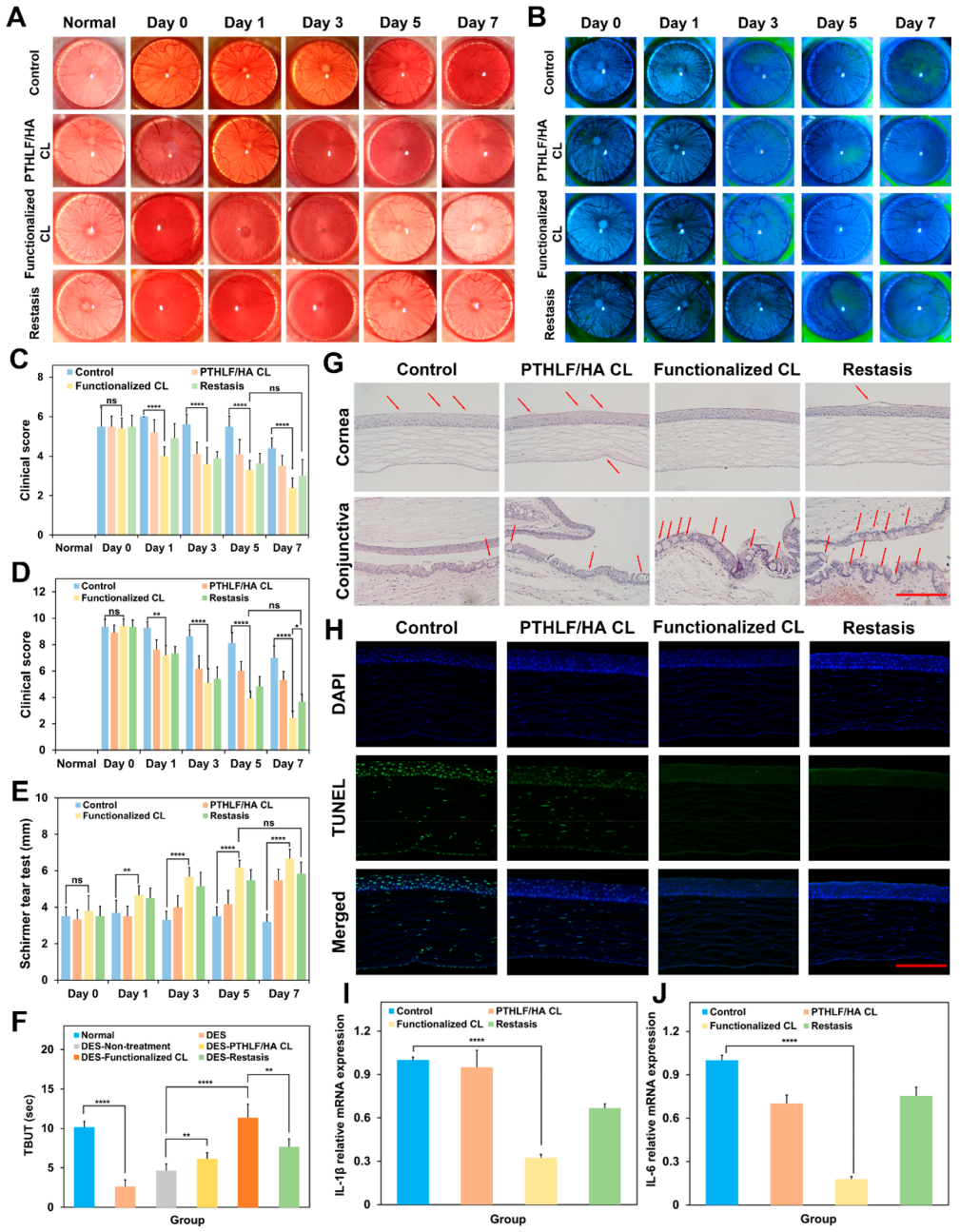

Figure 6. *In vivo* evaluation of the DES SD rats model after different intervention treatments. Representative slit lamp field images (A) and corresponding anterior segment clinical scores (C) of SD rats at 0, 1, 3, 5, and 7 days after various treatments with the untreated control, PTHLF/HA film-coated CL, functionalized nanofilm (21 μg)-coated CL, and Restasis. Representative post-treatment images of corneal fluorescein staining (B) and clinical scores (D) at 0, 1, 3, 5, and 7 days after various treatments. (E) STT (Schirmer tear test) scores of SD rats at 0, 1, 3, 5, and 7 days after various treatments. (F) TBUT of normal SD rats, DES SD rats at 0 days, DES SD rats without treatments after 7 days, and DES SD rats with various treatments after 7 days. (G) Representative immunohistochemical analysis images of the cornea and conjunctiva at 7 days after various treatments. The scale bar is 150 μm. (H) Representative images of the TUNEL staining of corneas at 7 days with various treatments. The scale bar is 150 μm. Expression of IL-1β (I) and IL-6 (J) mRNA in the corneas of SD rats at 7 days with various treatments. Statistical significance: $p < 0.01$ (*), $p < 0.001$ (**), $p < 0.0005$ (***), $p < 0.0001$ (****).

nm, which would not influence the vision of the wearer (Figure 4F).

Toward a daily disposable CL, the functionalized nanofilm after drug loading showed a slow, linear-like sustained release of CsA over 24 h with an initial burst in the early stage (Figure 4G and Figure S41). This release rate and the corresponding equilibrium concentration at a stable plateau varied depending on the initial loading mass of CsA (Figure 4G). The short initial burst may be due to the drug adsorbed on the surface of the functionalized nanofilm (Figure S36), and the long-term sustained release arose from the drug trapped inside the functionalized nanofilm. According to Restasis medication specifications, the minimum effective amount of CsA released per day (assuming the daily wearing time is 8 h) from a functionalized CL (assuming the bioavailability of drug is 50%, by referring to the currently known maximum bioavailability of drug delivered by a CL) should be 3 μg/day (Figure S42 and the red dotted line in Figure 4G). In this regard, 21 μg, as the

https://doi.org/10.1021/acscentsci.2c00151
ACS Cent. Sci. 2022, 8, 705−717

encapsulated drug mass in the PTHLF nanofilm, was high enough to maintain a continuous release of CsA of more than 3 μg/day (Figure 4G and Figure S41). This dose was 72% lower than the recommended application dose per day of Restasis drops. In contrast to CsA, HA (1000−1500 kDa) is a linear macromolecule that is easily entangled with unfolded protein molecules, thereby reducing its release ratio to 30% over 24 h (Figure S43). Delivering a relatively constant low dose of drug during the wearing of a functionalized CL would effectively prevent large fluctuations in the ocular drug concentration and possible side effects from a high dose of CsA, such as ocular pain, burning sensation, hyperemia, renal toxicity, and gingival overgrowth.

Biocompatibility Evaluation of the Functionalized CL. Consistent with previous protein phase transition systems,[21,29] the good biocompatibility of the functionalized PTHLF nanofilm was further reflected by the Cell Counting Kit-8 (CCK-8) assay of human corneal epithelial cells (HCECs) and rat fibroblasts (L929 cells) (Figure S44A,B). In general, a cell viability greater than 90% was observed after the culture of HCECs for 2, 4, 7, and 10 h on 96-well plates containing different samples, including the PTHLF nanofilm, HA-loaded PTHLF (PTHLF/HA) nanofilm, and functionalized (PTHLF/HA/CsA with a loading of 21, 22, 25, 34, and 49 μg CsA) nanofilm-coated cell slides (Figure S44A). L929 cell viability was also tested, and the results were basically similar to those of HCECs (Figure S44B). Fluorescence microscopy was further used to visually evaluate the HCECs viability after coincubation with functionalized nanofilms (a loading of 0, 21, 22, 25, 34, and 49 μg CsA) for 2, 4, 7, and 10 h, which showed that the number of dead cells was very low and that the HCECs maintained high viability (Figure S44C). The above results suggested that the harmful effects of the functionalized PTHLF nanofilm on mammalian cells were negligible, demonstrating good safety in ocular surface applications.

The *in vivo* biocompatibility of the functionalized CL in the eyes of normal Sprague−Dawley rats (SD rats) was further evaluated. After wearing functionalized CLs with different drug loadings, it was found that the symptoms of ocular surface irritation in rats wearing the functionalized CLs were not obvious by observing the changes in the cornea, conjunctiva, atria, and iris (Figure 5A). However, mild ocular surface inflammation was observed in rats wearing the commercial CL (Figure 5A). The corneal fluorescein sodium staining results showed that the corneal epithelium of rats in all of the groups was intact, with a clear structure and no obvious damage (Figure 5B). Due to the good biocompatibility of PTHLF, the functionalized nanofilm did not increase the irritation and inflammation of the tissue while improving the biocompatibility of the pristine CL to reduce inflammation on the ocular surface.[49] In this process, the functionalized CL played two important roles: effective suppressor of lacrimal protein adsorption and promoter of the controllable release of CsA. The clinical inflammation score (Table S2) and the fluorescein sodium staining score (Table S3) further confirmed the results (Figure 5C,D). The clinical inflammation score was based on anterior segment inflammation, including the structure of the conjunctiva, cornea, atria, and iris, and the fluorescein sodium staining score was based on the degree of corneal epithelial defect. The corneal tissue sections after hematoxylin-eosin staining (H&E) showed that the corneal structure in each group was clear and complete, and the corneal epithelial cells were arranged neatly without obvious defects (Figure 5E). The results of TdT-mediated dUTP nick-end labeling (TUNEL) staining also proved the good condition of the corneal epithelial cells in each group, and no apoptosis occurred (Figure 5F).

***In Vivo* Therapeutic Efficacy of the Functionalized CL.** A controllable release of CsA at a low dose from a biocompatible CL is promising to achieve improved therapeutic efficacy for DES treatment. To prove this improved efficacy, a functionalized CL with a drug loading of 21 μg was then used to conduct an *in vivo* DES treatment. The DES model in rats was established to evaluate the therapeutic efficacy of the functionalized CL. According to the bright field pictures of the slit lamp, the DES model rats showed obvious corneal roughness, conjunctival hyperemia, and iris hyperemia on the ocular surface compared with normal rats (Figure 6A). As observed by corneal fluorescein staining, there was a large amount of fluorescein sodium on the ocular surface of DES model rats, indicating damage to the corneal epithelium (Figure 6B). Regarding therapeutic intervention, ocular surface inflammation was significantly reduced in the functionalized CL and Restasis groups with clear and transparent corneas as well as significantly decreased conjunctiva and iris hyperemia (Figure 6A). Furthermore, the strength of corneal fluorescein sodium staining significantly decreased, indicating the gradual repair of the corneal epithelium (Figure 6B). It was also found that the inflammatory response in the PTHLF/HA CL group obviously decreased, which could be due to the enhanced tear stability, decreased tear flow rate, and anti-adhesion of the proteins in the HA component.[50] The clinical ocular surface inflammation scores and corneal fluorescein sodium staining scores in each group further showed that the functionalized CL had a much better effect during DES treatment than the clinical product Restasis (Figure 6C,D). The above results indicated the excellent therapeutic efficacy of the functionalized CL in improving ocular surface inflammation and in accelerating the repair of corneal epithelial deficiency. DES causes instability of the tear film, which affects the tear content on the ocular surface.[51,52] As the content of tears continues to decrease, symptoms such as corneal dryness and tingling develop, followed by corneal epithelial deficiency and normal corneal physiological structure damage. Therefore, the tear content on the ocular surface can reflect the severity of DES. As shown in Figure 6E, the tear content on the ocular surface of the DES model rats was very low. As the treatment progressed, the tear content gradually increased in the intervention treatment groups, including the PTHLF/HA CL, functionalized CL, and Restasis groups, which was significantly different from that in the control group. In particular, the rats in the functionalized CL group showed the best recovery of tear content after 5 days of intervention treatment, which was even higher than that in the Restasis group after 7 days of intervention. The tear film breakup time (TBUT) test, the most intuitive and accurate verification method for the stability of the tear film,[43] also showed that the TBUT of DES rats greatly improved after different intervention treatments for 7 days (Figure 6F). The TBUT of rats in the functionalized CL group exhibited the greatest increase, which was even slightly longer than that of normal rats, while the TBUT of rats in the Restasis group did not recover to normal rats. The above results indicated that compared to Restasis, the functionalized CL provided much better therapeutic efficacy in improving the stability of the tear film and maintaining the level of tears on the ocular surface.

https://doi.org/10.1021/acscentsci.2c00151
ACS Cent. Sci. 2022, 8, 705−717

Pathological changes in the rat cornea were further revealed through the H&E staining of corneal tissue (Figure 6G) and TUNEL cell apoptosis experiments (Figure 6H). As shown in Figure 6G, in the DES group without any intervention, the corneal epithelium was obviously damaged, the arrangement of the corneal epithelial cells was disordered, and the number of the conjunctival goblet cells was greatly reduced, indicating the development of severe DES. After 7 days of treatment with functionalized CL, the structure of the corneal epithelium of the DES rats was tight, the corneal epithelial cells were arranged neatly, and the number of conjunctival goblet cells increased significantly. Regarding the DES rats treated with PTHLF/HA CL and Restasis, the number of conjunctival goblet cells in the DES rats also increased, but there were still some obvious corneal epithelial deficiencies. In the TUNEL experiment, a large amount of corneal epithelial cell apoptosis was observed in the untreated or PTHLF/HA CL-treated groups, while no obvious apoptosis was found in the other two groups, indicating excellent therapeutic effects (Figure 6H). The above results then indicated that the drug loaded in the functionalized CL, which had a much lower loading dose of CsA than Restasis, showed excellent therapeutic effect for the repair of corneal epithelial deficiency and increased the number of conjunctival goblet cells. Furthermore, as reflected by real-time quantitative polymerase chain reaction (RT-qPCR), the mRNA expression levels of inflammatory factors in the functionalized CL group, including IL-1β (Figure 6I) and IL-6 (Figure 6J), were significantly lower than those in the Restasis and PTHLF/HA CL groups.

Overall, the functionalized CL demonstrated much better efficacy for DES treatment after five- and seven-day intervention than the Restasis group, which is based on the clinical ocular surface inflammation scores, corneal fluorescein sodium staining scores, and tear content on the ocular surface. The drug-loaded PTHLF nanofilm could deliver a relatively constant dose of drug during CL wearing, which would effectively prevent large fluctuations in the ocular drug concentration and possible side effects caused by Restasis eye drops. In addition, the increase in retention time of the drug on the ocular surface was also beneficial to increase the bioavailability of the drug, thus enhancing efficacy of the treatment. By comparing the amount of CsA used in the intervention treatments of the functionalized CL and Restasis, the bioavailability of CsA by the functionalized CL showed an 82% improvement over Restasis (the detailed calculation is described in the Supporting Information).

DISCUSSION

In this study, an amyloid-like nanofilm that can instantly form strong adhesion (within 2 s) on a hydrogel/tissue by fast amyloid-like protein aggregation is developed. Strong adhesion with the hydrogel/tissue surface is attributed to the various functional groups simultaneously exposed on the PTHLF nanofilm surface, especially the large number of hydrophobic groups, which effectively break through the hydration layer of the hydrogel/tissue surface. The PTHLF nanofilm, without any intrinsic color, displays excellent optical transparency and can be a unique class of stealth coating on hydrogel/tissue surfaces. The coating shows robust durability under harsh conditions, such as water scouring and the presence of surfactants, organic solvents, and extreme pH values. The nanofilm offers a biocompatible platform for encapsulating a high-density array of functional molecules such as CsA and HA with significant medicinal value. Moreover, the nanofilm has a pore size distribution of approximately 2 nm, which allows for the on-demand size-selective release of active molecules from the nanofilm. The functionalized CL prepared by the adhesion of drug-loaded nanofilms displays excellent therapeutic efficacy for *in vivo* DES treatment. The resultant bioavailability of CsA specifically for DES delivered by the functionalized CL is improved by at least 82% compared with Restasis, which is currently the only pharmacologic treatment approved by the US FDA. The reduced dose of CsA can decrease or prevent ocular surface irritation and systemic side effects (e.g., CsA-induced renal toxicity and gingival overgrowth), while patient compliance with the treatment regimen increases. The modification of hydrogel/tissue surfaces by the instant adhesion of the amyloid-like nanofilm provides new opportunities for drug delivery toward ophthalmology treatment, biocompatible wearable CL electronics, and hydrogel-based materials/devices.

In nature, several marine organisms, typically mussels, barnacles, and marine flatworms, have already utilized adhesive proteins for wet adhesion onto hydrophilic minerals in sea habitats. However, it remains largely unknown how adhesive proteins overcome the surface-bound water layer to establish underwater adhesion. In this regard, our present findings demonstrate that a biomimetic design of amyloid-like protein aggregates shows promise for achieving durable adhesion on wet surfaces, in which the hydrophobic side chains of proteins may be a critical component.[36,37]

METHODS

Preparation of the PTHLF Nanofilm. The phase transition solution containing HLF was freshly prepared by mixing a stock solution of HLF (7 mg/mL in Milli-Q water at pH 6.2) with TCEP solution (50 mM TCEP in Milli-Q water at pH 7.0) at a volume ratio of 1:1. The protein phase transition solution was dropped on a piece of glass (e.g., 18 × 18 mm^2), and then the solution on the substrate was incubated in a humid environment (generally for 2−6 h) at room temperature. The phase transition of HLF was initiated spontaneously upon mixing, and a nanofilm of the PTHLF product was formed at the solution surface.

Preparation of the Functionalized PTHLF Nanofilm. The phase transition solution was freshly prepared by mixing a stock solution of HLF (7 mg/mL in Milli-Q water at pH 6.2), HA solution (6/9/12 mg/mL in Milli-Q water), TCEP solution (50 mM TCEP in Milli-Q water at pH 7.0), and CsA solution (7.5 mg/mL in aqueous ethanol, 50% by volume) at a volume ratio of 15:15:15:n (n = 1, 2, 3, 4, 5, 6). The solution was dropped on a piece of glass (e.g., 18 × 18 mm^2) and then incubated in a humid environment (generally for 6−12 h) at room temperature.

Peeling Test. Unless otherwise stated, all nanofilm-coated hydrogel/tissue samples were stored at 4 °C in water for 24 h to ensure an equilibrium swelling state of the nanofilm-coated hydrogel/tissue before being tested. All tests were performed in an ambient environment at room temperature. The hydrogel and nanofilm-coated hydrogel maintained consistent properties over the duration of the tests (that is, approximately a few minutes), during which the effect of dehydration was not significant. The peeling strength measurement was carried out using a DCAT 21 apparatus (Figure S20). To maintain a constant contact area in each test, a copper plate (0.5 cm × 0.5 cm) with 0.1 μL tissue adhesive Histoacryl (consisting of *n*-

https://doi.org/10.1021/acscentsci.2c00151
ACS Cent. Sci. 2022, 8, 705−717

butyl-2-cyanoacrylate) was used as a substrate to contact the nanofilm-coated hydrogel/tissue. To make it easier to confirm that only the nanofilm was completely peeled off from the hydrogel/tissue, the following method was used: (i) before modifying the different hydrogel/tissue samples, the nanofilm was dyed by 0.1 wt % Congo red with the method in Figure S17; (ii) before applying the Histoacryl onto the copper plate, a layer of single-sided tape was attached to the copper plate (0.5 cm × 0.5 cm), and then a layer of double-sided tape was attached; after the measurement was finished, all of the tape was peeled off from the copper plate and the nanofilm peeled from the hydrogel/tissue could be seen very clearly against the white background (Figure S20C).

At the start of the test, the scale was automatically tared to zero, under which the forces exerted on the copper plate were balanced. Then, the nanofilm-coated hydrogel/tissue was driven upward by a micromotor to contact the copper plate. Once the copper plate contacted the nanofilm-coated hydrogel/tissue, the motor was set to move upward another 2 mm at a speed of 0.2 mm/s to achieve sufficient interaction between the Histoacryl and nanofilm-coated hydrogel/tissue; then, the motor was set to move downward at the same speed, resulting in the separation of the nanofilm and the hydrogel/tissue. At the critical point of complete separation, the peak indicated the adhesion force between the nanofilm and the hydrogel/tissue. A typical weight-versus-distance curve was recorded throughout the approach−contact−separation process. The peeling strength was calculated by the following equation:

$$\text{Peeling strength} = \frac{m \times g}{S}$$

where m is the peak of the weight-versus-distance curve, g is the gravitational acceleration, and S is the contact area between the copper plate and nanofilm-coated hydrogel/tissue (0.25 cm^2).

To ensure the accuracy of the peeling strength and verify that no Histoacryl penetrated into and interacted with the hydrogel/tissue during the peeling experiment, Histoacryl mixed with 0.1 wt % ThT dye (dissolved in ethanol) was used to interact with the nanofilm-coated hydrogel/tissue. After the peeling experiment was completed, macroscopic (the sample under 488 nm laser irradiation) and microscopic (LSCM) fluorescence testing were performed on the nanofilm-coated hydrogel and the peeled nanofilm (Figure S21). The results showed that there was no fluorescence of the nanofilm-coated hydrogel after the peeling test, indicating that Histoacryl did not penetrate into the hydrogel and only interacted with the nanofilm during the peeling test.

Water Scouring Test. To avoid washing away the sample under water flow, the nanofilm-coated PHEMA hydrogel was attached to a Petri dish, and the Petri dish was attached to a metal plate (20 cm × 30 cm). The samples were stored at 4 °C in water for 24 h to ensure equilibrium swelling state before the test.

The setup shown in Figure S24A was used to test the force between the water flow and nanofilm-coated PHEMA hydrogel. Because the distance between the nanofilm-coated hydrogels and the water outlet was very short (~10 cm), it was assumed that there was no change in the water flow velocity or cross-sectional area. Therefore, the calculation formula of the flushing force (**F**) between the water flow and nanofilm-coated PHEMA hydrogel is given as follows:

$$\mathbf{F} = (P_c - P_t) \times S$$

where P_c (0.2 MPa) and P_t (0 MPa) are the pressures when the water valve is closed and the test is carried out, respectively, and S (0.16π cm^2) is the cross-sectional area of the pipeline. Therefore, the flushing force (**F**) between the water flow and the nanofilm-coated PHEMA hydrogel was calculated to be 10.05 N.

Preparation of the Functionalized CL. This experiment was carried out on a sterile operating table. The CL was a commercial EASY DAY (Hydron, USA). The CL was immersed in Milli-Q water for 2 h to remove impurities before modification with the functionalized PTHLF nanofilm. The HLF, TCEP, CsA, and HA solutions, used to prepare the functionalized PTHLF nanofilms, were filtered and sterilized through a 0.22 μm filter. The functionalized CL was prepared by adhering the functionalized nanofilm on the CL and rinsing with Milli-Q water three times. The functionalized CL was then placed in a wet CL box, sealed with sealing film, and stored at 4 °C for subsequent experiments.

***In Vitro/Vivo* Biocompatibility and *In Vivo* Intervention Tests.** Details of the *in vitro* biological safety test and *in vivo* intervention are provided in the Supporting Information.

Safety Statement. No unexpected or unusually high safety hazards were encountered.

■ ASSOCIATED CONTENT

Supporting Information

The Supporting Information is available free of charge at https://pubs.acs.org/doi/10.1021/acscentsci.2c00151.

Detailed experimental methods and results (PDF)
Instant adhesion of nanofilm with different hydrogel surface (AVI)
Instant adhesion of nanofilm with different hydrogel surface (AVI)
Instant adhesion of nanofilm with different hydrogel surface (AVI)
Instant adhesion of nanofilm with different hydrogel surface (AVI)
Instant adhesion of nanofilm with different hydrogel surface (AVI)
Peeling test of PTHLF nanofilm-coated AG hydrogel (AVI)

■ AUTHOR INFORMATION

Corresponding Authors

Peng Yang − *Key Laboratory of Applied Surface and Colloid Chemistry, Ministry of Education, School of Chemistry and Chemical Engineering, Shaanxi Normal University, Xi'an 710119, China;* orcid.org/0000-0002-0463-1024; Email: yangpeng@snnu.edu.cn

Bailiang Wang − *School of Ophthalmology & Optometry, Eye Hospital, Wenzhou Medical University, Wenzhou 325027, China*; Email: blwang@wmu.edu.cn

Authors

Rongrong Qin − *Key Laboratory of Applied Surface and Colloid Chemistry, Ministry of Education, School of Chemistry and Chemical Engineering, Shaanxi Normal University, Xi'an 710119, China*

Yishun Guo − *School of Ophthalmology & Optometry, Eye Hospital, Wenzhou Medical University, Wenzhou 325027, China*

https://doi.org/10.1021/acscentsci.2c00151
ACS Cent. Sci. 2022, 8, 705−717

Hao Ren − *Key Laboratory of Applied Surface and Colloid Chemistry, Ministry of Education, School of Chemistry and Chemical Engineering, Shaanxi Normal University, Xi'an 710119, China*

Yongchun Liu − *Key Laboratory of Applied Surface and Colloid Chemistry, Ministry of Education, School of Chemistry and Chemical Engineering, Shaanxi Normal University, Xi'an 710119, China;* orcid.org/0000-0001-9212-8439

Hao Su − *Key Laboratory of Applied Surface and Colloid Chemistry, Ministry of Education, School of Chemistry and Chemical Engineering, Shaanxi Normal University, Xi'an 710119, China*

Xiaoying Chu − *School of Ophthalmology & Optometry, Eye Hospital, Wenzhou Medical University, Wenzhou 325027, China*

Yingying Jin − *School of Ophthalmology & Optometry, Eye Hospital, Wenzhou Medical University, Wenzhou 325027, China*

Fan Lu − *School of Ophthalmology & Optometry, Eye Hospital, Wenzhou Medical University, Wenzhou 325027, China*

Complete contact information is available at: https://pubs.acs.org/10.1021/acscentsci.2c00151

Author Contributions

#P.Y., B.W., R.Q., and Y.G. conceived and designed the experiments. R.Q. performed the material preparations, characterization, and in vitro released experiments with input from H. S. Y.G. conducted the experiments of cell and animal experiments with input from X.C., Y.J., and F.L. R.Q. analyzed MD simulations data with input from Y.L. and R.H. R.Q., Y.G., B.W., and P.Y. wrote the paper. All authors have given approval to the final version of the manuscript. R.Q. and Y.G. contributed equally.

Notes

The authors declare no competing financial interest.

■ ACKNOWLEDGMENTS

P.Y. thanks the funding from the National Key R&D Program of China (nos. 2020YFA0710400, 2020YFA0710402), the National Natural Science Foundation of China (nos. 21875132, 51903147, 21905166), the 111 Project (no. B14041), the Fundamental Research Funds for the Central Universities (2020TS092), and the Innovation Capability Support Program of Shaanxi (no. 2020TD024). B.W. thanks the funding from the Zhejiang Provincial Natural Science Foundation of China (LR21H180001), Project of State Key Laboratory of Ophthalmology, Optometry and Visual Science, Wenzhou Medical University (J02-20190203), Wenzhou key program of scientific and technological innovation (ZY2019017), and National Key R&D Program of China, (No. 2020YFC2008200), Zhejiang Provincial Traditional Chinese Medicine Science and Technology Project (2021ZA091).

■ REFERENCES

(1) Lee, H.; Dellatore, S. M.; Miller, W. M.; Messersmith, P. B. Mussel-inspired surface chemistry for multifunctional coatings. *Science* **2007**, *318*, 426−430.

(2) Ejima, H.; Richardson, J. J.; Liang, K.; Best, J. P.; van Koeverden, M. P.; Such, G. K.; Cui, J.; Caruso, F. One-step assembly of coordination complexes for versatile film and particle engineering. *Science* **2013**, *341*, 154−157.

(3) Rapp, M. V.; Maier, G. P.; Dobbs, H. A.; Higdon, N. J.; Waite, J. H.; Butler, A.; Israelachvili, J. N. Defining the catechol-cation synergy for enhanced wet adhesion to mineral surfaces. *J. Am. Chem. Soc.* **2016**, *138*, 9013−9016.

(4) Yao, X.; Chen, L.; Ju, J.; Li, C.; Tian, Y.; Jiang, L. Superhydrophobic diffusion barriers for hydrogels via confined interfacial modification. *Adv. Mater.* **2016**, *28*, 7383−7389.

(5) Khalil, I. A.; Saleh, B.; Ibrahim, D. M.; Jumelle, C.; Yung, A.; Dana, R.; Annabi, N. Ciprofloxacin-loaded bioadhesive hydrogels for ocular applications. *Biomater. Sci.* **2020**, *8*, 5196.

(6) Hu, X.; Tan, H.; Wang, X.; Chen, P. Surface functionalization of hydrogel by thiol-yne click chemistry for drug delivery. *Colloids and Surfaces A: Physicochem. Eng. Aspects.* **2016**, *489*, 297−304.

(7) Wang, Y.; Shang, L.; Chen, G.; Sun, L.; Zhang, X.; Zhao, Y. Bioinspired structural color patch with anisotropic surface adhesion. *Sci. Adv.* **2020**, *6*, No. eaax8258.

(8) Jeong, J. W.; McCall, J. G.; Shin, G.; Zhang, Y.; Al-Hasani, R.; Kim, M.; Li, S.; Sim, J. Y.; Jang, K. I.; Shi, Y.; et al. Wireless optofluidic systems for programmable *in vivo* pharmacology and optogenetics. *Cell* **2015**, *162*, 662−674.

(9) Jungnickel, C.; Tsurkan, M. V.; Wogan, K.; Werner, C.; Schlierf, M. Bottom-up structuring and site-selective modification of hydrogels using a two-photon [2 + 2] cycloaddition of maleimide. *Adv. Mater.* **2017**, *29*, 1603327.

(10) Yuk, H.; Zhang, T.; Parada, G. A.; Liu, X.; Zhao, X. Skin-inspired hydrogel-elastomer hybrids with robust interfaces and functional microstructures. *Nat. Commun.* **2016**, *7*, 12028.

(11) Xu, S.; Zhang, Y.; Jia, L.; Mathewson, K. E.; Jang, K. I.; Kim, J.; Fu, H.; Huang, X.; Chava, P.; Wang, R.; et al. Soft microfluidic assemblies of sensors, circuits, and radios for the skin. *Science* **2014**, *344*, 70−74.

(12) Morin, S. A.; Shepherd, R. F.; Kwok, S. W.; Stokes, A. A.; Nemiroski, A.; Whitesides, G. M. Camouflage and display for soft machines. *Science* **2012**, *337*, 828−832.

(13) Wan, X.; Xu, X.; Liu, X.; Jia, L.; He, X.; Wang, S. A wetting-enabled-transfer (wet) strategy for precise surface patterning of organohydrogels. *Adv. Mater.* **2021**, *33*, 2008557.

(14) Xu, C.; He, R.; Xie, B.; Ismail, M.; Yao, C.; Luan, J.; Li, X. Silicone hydrogels grafted with natural amino acids for ophthalmological application. *J. Biomat. Sci. Polym. Ed.* **2016**, *27*, 1354−1368.

(15) Yao, X.; Liu, J.; Yang, C.; Yang, X.; Wei, J.; Xia, Y.; Gong, X.; Suo, Z. Hydrogel paint. *Adv. Mater.* **2019**, *31*, 1903062.

(16) Liu, J.; Qu, S.; Suo, Z.; Yang, W. Functional hydrogel coatings. *Natl. Sci. Rev.* **2021**, *8*, No. nwaa254.

(17) Zhang, D.; Liu, J.; Chen, Q.; Jiang, W.; Wang, Y.; Xie, J.; Ma, K.; Shi, C.; Zhang, H.; Chen, M.; et al. A sandcastle worm-inspired strategy to functionalize wet hydrogels. *Nat. Commun.* **2021**, *12*, 6331.

(18) So, C. R.; Yates, E. A.; Estrella, L. A.; Fears, K. P.; Schenck, A. M.; Yip, C. M.; Wahl, K. J. Molecular recognition of structures is key in the polymerization of patterned barnacle adhesive sequences. *ACS Nano* **2019**, *13*, 5172−5183.

(19) Wang, D.; Ha, Y.; Gu, J.; Li, Q.; Zhang, L.; Yang, P. 2D protein supramolecular nanofilm with exceptionally large area and emergent functions. *Adv. Mater.* **2016**, *28*, 7414−7423.

(20) Li, C.; Xu, L.; Zuo, Y.; Yang, P. Tuning protein assembly pathways through superfast amyloid-like aggregation. *Biomater. Sci.* **2018**, *6*, 836−841.

(21) Hu, X.; Tian, J.; Li, C.; Su, H.; Qin, R.; Wang, Y.; Cao, X.; Yang, P. Amyloid-like protein aggregates: a new class of bioinspired materials merging an interfacial anchor with antifouling. *Adv. Mater.* **2020**, *32*, 2000128.

(22) Baker, E. N.; Baker, H. M. A structural framework for understanding the multifunctional character of lactoferrin. *Biochimie* **2009**, *91*, 3−10.

(23) Anderson, B. F.; Baker, H. M.; Norris, G. E.; Rice, D. W.; Baker, E. N. Structure of human lactoferrin: crystallographic structure

analysis and refinement at 2.8 Å resolution. *J. Mol. Biol.* **1989**, *209*, 711−734.
(24) Sun, X. L.; Baker, H. M.; Shewry, S. C.; Jameson, G. B.; Baker, E. N. Structure of recombinant human lactoferrin expressed in *aspergillus awamori*. *Acta Crystallogr.* **1999**, *D55*, 403−407.
(25) Yavuz, B.; Bozdag, P. S.; Unlu, N. An overview on dry eye treatment: approaches for cyclosporin A delivery. *Sci. World J.* **2012**, *2012*, 194848.
(26) Guzman-Aranguez, A.; Fonseca, B.; Carracedo, G.; Martin-Gil, A.; Martinez-Aguila, A.; Pintor, J. Dry eye treatment based on contact lens drug delivery: A review. *Eye Contact Lens.* **2016**, *42*, 280−288.
(27) Liu, Y.; Tao, F.; Miao, S.; Yang, P. Controlling the Structure and Function of Protein Thin Films through Amyloid-Like Aggregation. *Acc. Chem. Res.* **2021**, *54*, 3016−3027.
(28) Chimon, S.; Ishii, Y. Capturing intermediate structures of alzheimer's β-amyloid, Aβ(1−40), by solid-state NMR spectroscopy. *J. Am. Chem. Soc.* **2005**, *127*, 13472−13473.
(29) Gu, J.; Su, Y.; Liu, P.; Li, P.; Yang, P. An environmentally benign antimicrobial coating based on a protein supramolecular assembly. *ACS Appl. Mater. Interfaces* **2017**, *9*, 198−210.
(30) Xu, Y.; Liu, Y.; Hu, X.; Qin, R.; Su, H.; Li, J.; Yang, P. Synthesis of 2D ultralarge protein supramolecular nanofilm by chemoselective thiol-disulfide exchange and emergent functions. *Angew. Chem., Int. Ed.* **2020**, *59*, 2850−2859.
(31) Barlow, D. E.; Dickinson, G. H.; Orihuela, B.; Kulp, J. L.; Rittschof, D.; Wahl, K. J. Characterization of the adhesive plaque of the barnacle balanus amphitrite: amyloid-like nanofibrils are a major component. *Langmuir* **2010**, *26*, 6549−6556.
(32) Alsteens, D.; Ramsook, C. B.; Lipke, P. N.; Dufrêne, Y. F. Unzipping a functional microbial amyloid. *ACS Nano* **2012**, *6*, 7703−7711.
(33) Gu, J.; Miao, S.; Yan, Z.; Yang, P. Multiplex binding of amyloid-like protein nanofilm to different material surfaces. *Colloids Interface Sci. Commun.* **2018**, *22*, 42−48.
(34) Israelachvili, J.; Wennerstrom, H. Role of hydration and water structure in biological and colloidal interactions. *Nature* **1996**, *379*, 219−25.
(35) Pashley, R. M. Hydration forces between mica surfaces in electrolyte solutions. *Adv. Colloid Interface Sci.* **1982**, *16*, 57−62.
(36) Yu, J.; Kan, Y.; Rapp, M.; Danner, E.; Wei, W.; Das, S.; Miller, D. R.; Chen, Y.; Waite, J. H.; Israelachvili, J. N. Adaptive hydrophobic and hydrophilic interactions of mussel foot proteins with organic thin films. *Proc. Natl. Acad. Sci. U. S. A.* **2013**, *110*, 15680−15685.
(37) Akdogan, Y.; Wei, W.; Huang, K.; Kageyama, Y.; Danner, E. W.; Miller, D. R.; Rodriguez, N. R. M.; Waite, J. H.; Han, S. Intrinsic surface-drying properties of bioadhesive proteins. *Angew. Chem., Int. Ed.* **2014**, *126*, 11435−11438.
(38) Du, Q.; Freysz, E.; Shen, Y. R. Surface vibrational spectroscopic studies of hydrogen bonding and hydrophobicity. *Science* **1994**, *264*, 826−828.
(39) Joesten, M. D.; Schaad, L. J. *Hydrogen Bonding*; Marcel Dekker Inc., New York, USA, 1974.
(40) Li, J.; Tian, J.; Gao, Y.; Qin, R.; Pi, H.; Li, M.; Yang, P. All-natural superhydrophobic coating for packaging and blood-repelling materials. *Chem. Eng. J.* **2021**, *410*, 128347.
(41) Pillar, S.; Almog, Y.; Sharon, T.; Dar, N.; Segal, O.; Nemet, A. Y. Objective measurement of eyelid force in ptosis versus controls. *J. Craniofac. Surg.* **2019**, *30*, 2533−2535.
(42) Kim, J.; Kim, M.; Lee, M. S.; Kim, K.; Ji, S.; Kim, Y. T.; Park, J.; Na, K.; Bae, K. H.; Kim, H. K.; et al. Wearable smart sensor systems integrated on soft contact lenses for wireless ocular diagnostics. *Nat. Commun.* **2017**, *8*, 14997.
(43) Peng, C. C.; Chauhan, A. Extended cyclosporine delivery by silicone-hydrogel contact lenses. *J. Controlled Release* **2011**, *154*, 267−274.
(44) Kapoor, Y.; Thomas, J. C.; Tan, G.; John, V. T.; Chauhan, A. Surfactant-laden soft contact lenses for extended delivery of ophthalmic drugs. *Biomaterials* **2009**, *30*, 867−878.
(45) Ali, M.; Byrne, M. E. Controlled release of high molecular weight hyaluronic acid from molecularly imprinted hydrogel contact lenses. *Pharm. Res.* **2009**, *26*, 714−726.
(46) Tieppo, A.; Pate, K. M.; Byrne, M. E. *In vitro* controlled release of an anti-inflammatory from daily disposable therapeutic contact lenses under physiological ocular tear flow. *Eur. J. Pharm. Biopharm.* **2012**, *81*, 170−177.
(47) Yu, F.; Zheng, M.; Zhang, A. Y.; Han, Z. A cerium oxide loaded glycol chitosan nano-system for the treatment of dry eye disease. *J. Controlled Release* **2019**, *315*, 40−54.
(48) Yang, F.; Tao, F.; Li, C.; Gao, L.; Yang, P. Self-assembled membrane composed of amyloid-like proteins for efficient size-selective molecular separation and dialysis. *Nat. Commun.* **2018**, *9*, 5443.
(49) Bischoff, G.; Kuhn, D. Contact lens complications: diagnosis and treatment. *Ophthalmologe* **2018**, *115*, 1087−1102.
(50) Ang, B. C. H.; Sng, J. J.; Wang, P. X. H.; Htoon, H. M.; Tong, L. H. T. Sodium hyaluronate in the treatment of dry eye syndrome: A systematic review and meta-analysis. *Sci. Rep.* **2017**, *7*, 9013.
(51) Lin, M. C.; Asbell, P. A.; Margolis, T.; McNamarra, N. A.; Nichols, K. K.; Nichols, J. J.; Polse, K. A. Dry eye disease. *Optom. Vis. Sci.* **2015**, *92*, 922−924.
(52) Bang, S. P.; Yeon, C. Y.; Adhikari, N.; Neupane, S.; Kim, H.; Lee, D. C.; Son, M. J.; Lee, H. G.; Kim, J. Y.; Jun, J. H. Cyclosporine A eyedrops with self-nanoemulsifying drug delivery systems have improved physicochemical properties and efficacy against dry eye disease in a murine dry eye model. *PLoS One* **2019**, *14*, No. e0224805.

https://doi.org/10.1021/acscentsci.2c00151
ACS Cent. Sci. 2022, 8, 705−717